



Supporting Information

for

Preparation of anthracene-based tetraaperimidine hexafluorophosphate and selective recognition of chromium(III) ions

Qing-Xiang Liu, Feng Yang, Zhi-Xiang Zhao, Shao-Cong Yu and Yue Ding

Beilstein J. Org. Chem. **2019**, *15*, 2847–2855. doi:10.3762/bjoc.15.278

Supporting crystallographic data, fluorescence, UV, HRMS, and IR spectra of 3 and 3·Cr³⁺, general considerations, characterization data, and copies of the ¹H and ¹³C NMR spectra of all compounds

Table of contents

1. CCDC numbers for compound **3**.
2. Crystal data and structure refinements for **3** (Table S1).
3. Crystal packing of compound **3** (Figure S1(a) and Figure S1(b)).
4. Fluorescence and UV–vis spectroscopy for compound **3** (Figures S2–S9).
5. Figure S10 π_{13}^{15} bond of perimidine.
6. Figure of HRMS for **3**·Cr³⁺ (Figure S11).
7. Infrared spectra of **3** and **3**·Cr³⁺ (Figure S12).
8. Figure of HRMS for **3** (Figure S13).
9. ¹H NMR and ¹³C NMR spectra of intermediate and compound **3** (Figures S14–S22).

1. CCDC number for compound 3.

CCDC 1918752 contains the supplementary crystallographic data for compound 3. The data can be obtained free of charge via <http://www.ccdc.cam.ac.uk/conts/retrieving.html>, or from the Cambridge Crystallographic Data Centre, 12 Union Road, Cambridge, CB2 1EZ, UK; fax: (+44) 223-336-033; or e-mail: deposit@ccdc.cam.ac.uk.

2. Crystal data and structure refinements for 3

Table S1: Crystal data and structure refinements for 3

Chemical formula	$C_{76}H_{76}N_{10}P_4F_{24} \cdot 4CH_3CN$	$F(000)$	968
Formula weight	1875.57	Cryst size, mm	$0.25 \times 0.15 \times 0.14$
Cryst syst	Triclinic	$\theta_{min}, \theta_{max}$, deg	3.74, 67.06
Space group	$P\bar{1}$	T/K	172.9(1)
$a/\text{\AA}$	11.850(5)	No. of data collected	14087
$b/\text{\AA}$	12.401(6)	No. of unique data	7439
$c/\text{\AA}$	14.951(5)	No. of refined params	579
α/deg	92.4(1)	Goodness-of-fit on F^2 ^a	1.048
β/deg	94.3(1)	Final R indices ^b [$I > 2\sigma(I)$]	
γ/deg	107.3(4)	R_1	0.0754
$V/\text{\AA}^3$	2086.65(1)	wR_2	0.1986
Z	1	R indices (all data)	
D_{calcd} , Mg/m ³	1.493	R_1	0.1117
Abs coeff, mm ⁻¹	1.797	wR_2	0.2238

^a $GOF = [\sum \omega(F_o^2 - F_c^2)^2 / (n - p)]^{1/2}$, where n is the number of reflection and p is the number of parameters refined. ^b $R_1 = \Sigma(|F_o| - |F_c|) / \Sigma|F_o|$; $wR_2 = [\Sigma[w(F_o^2 - F_c^2)^2] / \Sigma w(F_o^2)^2]^{1/2}$.

3. Crystal packing of compound 3

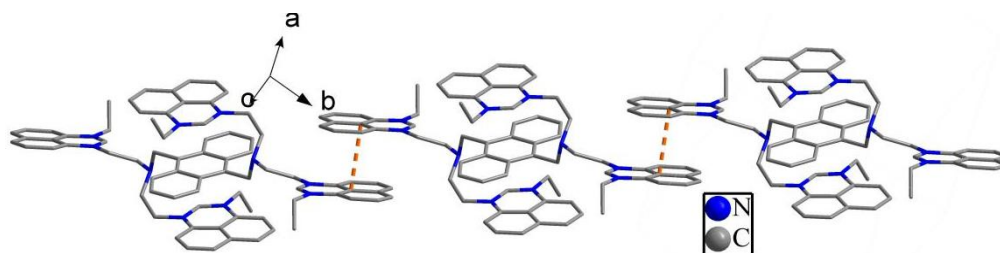


Figure S1(a): 1D supermolecular chain of **3**.

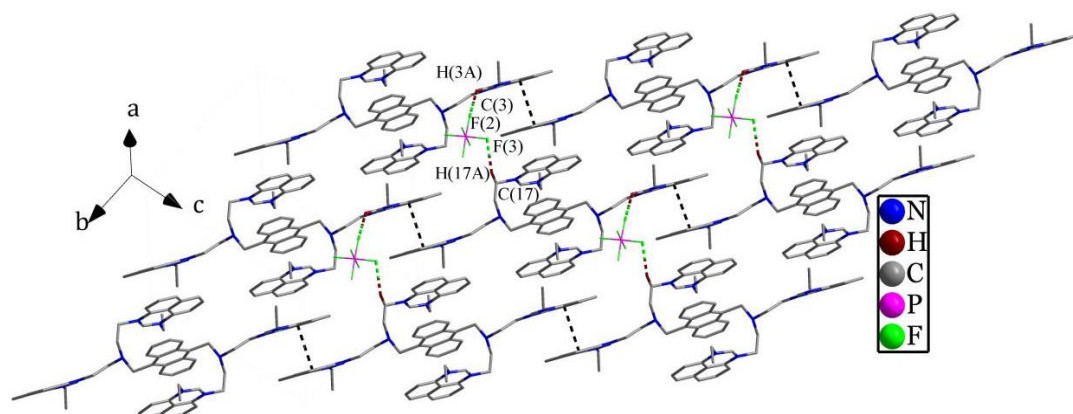


Figure S1(b): 2D supermolecular layer of **3**.

4. Fluorescence and UV-vis spectroscopy for compound 3

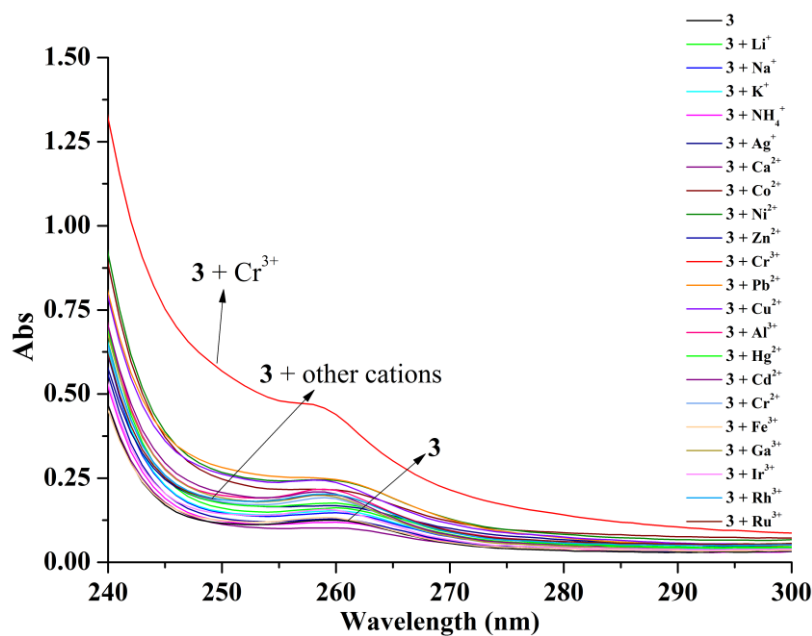


Figure S2: UV-vis absorption change of **3** (5.0×10^{-6} mol/L) upon the addition of the nitrate salts of K^+ , Na^+ , Li^+ , Ag^+ , NH_4^+ , Zn^{2+} , Cd^{2+} , Ca^{2+} , Ni^{2+} , Pb^{2+} , Cu^{2+} , Co^{2+} , Al^{3+} , Cr^{3+} , Hg^+ , Hg^{2+} , Rh^{3+} , Ir^{3+} , Cr^{2+} , Ga^{3+} , Ru^{3+} and Fe^{3+} (5×10^{-5} mol/L) in acetonitrile at 25 °C.

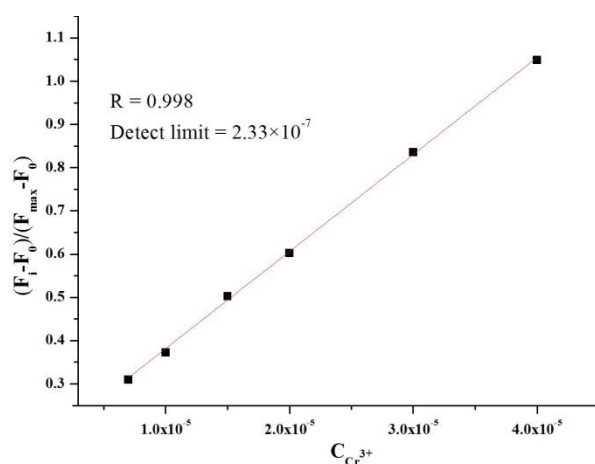


Figure S3: Emission (at 423 nm) of **3** at different concentrations of Cr^{3+} ($0.7, 1.0, 1.5, 2.0, 3.0, 4.0 \times 10^{-5}$ mol/L) added, normalized between the minimum emission (0.0 M Cr^{3+}) and the emission 4.0×10^{-5} mol/L Cr^{3+} . The detection limit was determined to be 2.33×10^{-7} mol/L.

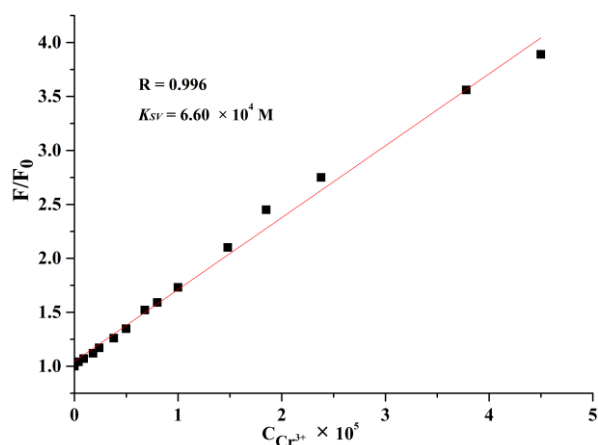


Figure S4: Stern–Volmer plot of **3** (5.0×10^{-6} mol/L) in the presence of Cr^{3+} in $\text{CH}_3\text{CN}/\text{DMSO}$ 9:1 (v:v) at 25°C , and the linear range is from 0.0 – 4.5×10^{-5} mol/L.

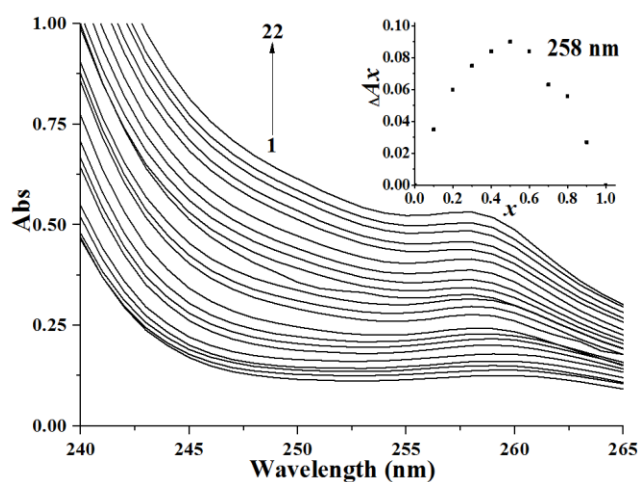


Figure S5: The UV–vis absorption spectra of **3** (5.0×10^{-6} mol/L) in $\text{CH}_3\text{CN}/\text{DMSO}$

9:1 (v/v) at 25 °C. $C_{Cr^{3+}}$ for curves 1–22 are 0, 0.02, 0.06, 0.1, 0.2, 0.4, 0.6, 0.8, 1.2, 1.4, 1.6, 1.8, 2.0, 2.2, 2.4, 2.6, 2.8, 3.0, 3.2, 3.4, 3.5 and 3.6×10^{-5} . Inset: the Job's plot for $3 \cdot Cr^{3+}$ complex in $CH_3CN/DMSO$ 9:1 (v/v) at 258 nm.

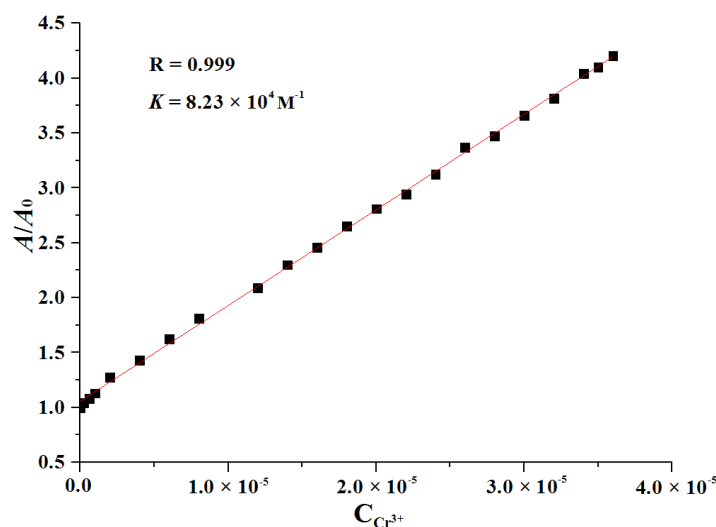


Figure S6: Benesi–Hildebrand plot of **3** (5.0×10^{-6} mol/L) at 258 nm in the presence of Cr^{3+} in $CH_3CN/DMSO$ 9:1 (v/v) at 25 °C.

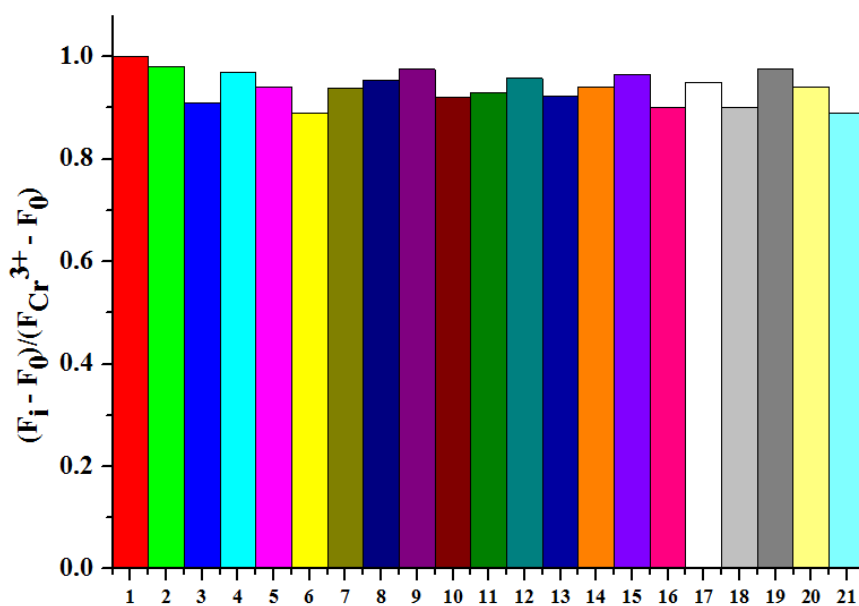


Figure S7: Change ratio $((F_i - F_0)/(F_{Cr^{3+}} - F_0))$ of fluorescence intensity of **3** (5.0×10^{-6} mol/L) at 423 nm upon the addition of 30 equiv Cr^{3+} in the presence of 30 equiv background cations. 1: Cr^{3+} ; 2: $Cr^{3+} + Li^+$; 3: $Cr^{3+} + Na^+$; 4: $Cr^{3+} + K^+$; 5: $Cr^{3+} + NH_4^+$; 6: $Cr^{3+} + Ag^+$; 7: $Cr^{3+} + Ca^{2+}$; 8: $Cr^{3+} + Co^{2+}$; 9: $Cr^{3+} + Ni^{2+}$; 10: $Cr^{3+} + Zn^{2+}$; 11: $Cr^{3+} + Cu^{2+}$; 12: $Cr^{3+} + Cd^{2+}$; 13: $Cr^{3+} + Pb^{2+}$; 14: $Cr^{3+} + Hg^{2+}$; 15: $Cr^{3+} + Al^{3+}$; 16: $Cr^{3+} +$

Rh^{3+} ; 17: $\text{Cr}^{3+} + \text{Ir}^{3+}$; 18: $\text{Cr}^{3+} + \text{Cr}^{2+}$; 19: $\text{Cr}^{3+} + \text{Ga}^{3+}$; 20: $\text{Cr}^{3+} + \text{Ru}^{3+}$; 21: $\text{Cr}^{3+} + \text{Fe}^{3+}$
in $\text{CH}_3\text{CN}/\text{DMSO}$ 9:1 (v/v) at 25 °C.

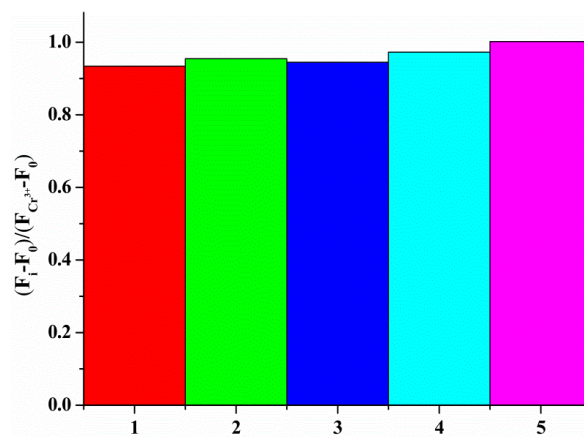


Figure S8: Fluorescence intensity of **3** (5.0×10^{-6} mol/L) in various mixtures of different Cr^{3+} salts (1: CrCl_3 , 2: CrBr_3 , 3: $\text{Cr}_2(\text{SO}_4)_3$, 4: $\text{Cr}(\text{OAc})_3$, 5: $\text{Cr}(\text{NO}_3)_3$; 3.0×10^{-6} mol/L) in $\text{CH}_3\text{CN}/\text{DMSO}$ 9:1 (v/v) at 25 °C.

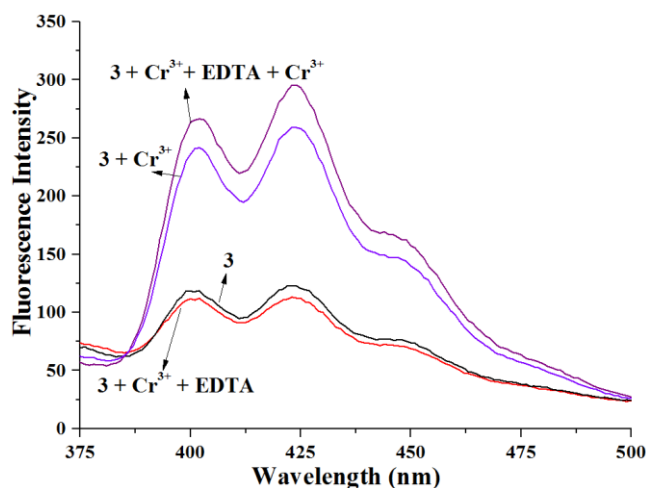


Figure S9: Fluorescence reversibility of **3** upon the detection of Cr^{3+} . Fluorescent changes of **3** after the addition of Cr^{3+} , EDTA, Cr^{3+} in that order in $\text{CH}_3\text{CN}/\text{DMSO}$ 9:1 (v/v) at 25 °C.

5. The Figure S10 π_{13}^{15} bond of perimidine

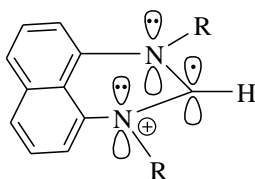


Figure S10: π_{13}^{15} bond of perimidine.

6. Figure of HRMS for $3 \cdot \text{Cr}^{3+}$

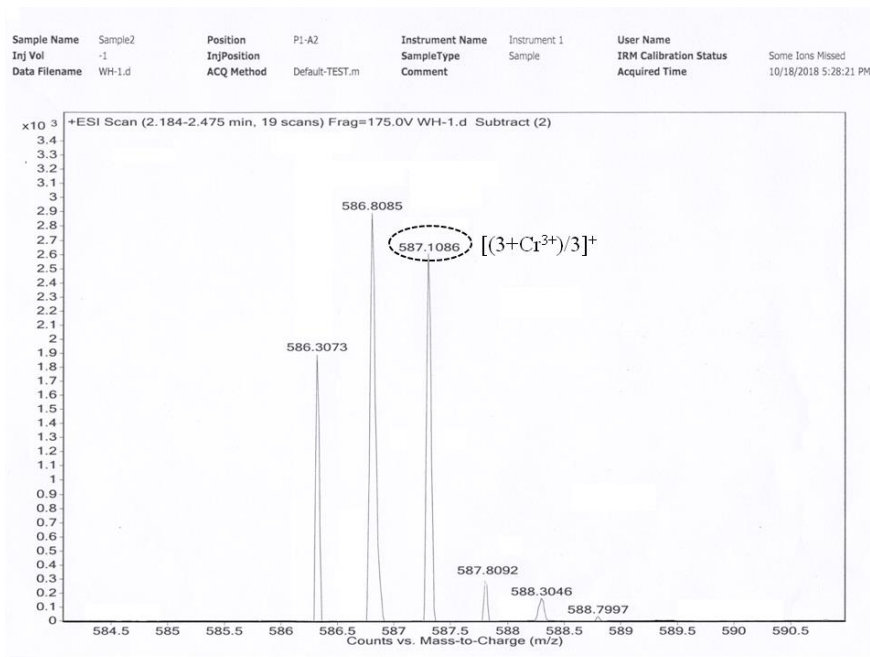


Figure S11: HRMS for $3 \cdot \text{Cr}^{3+}$.

7. Infrared spectra of **3** and $3 \cdot \text{Cr}^{3+}$

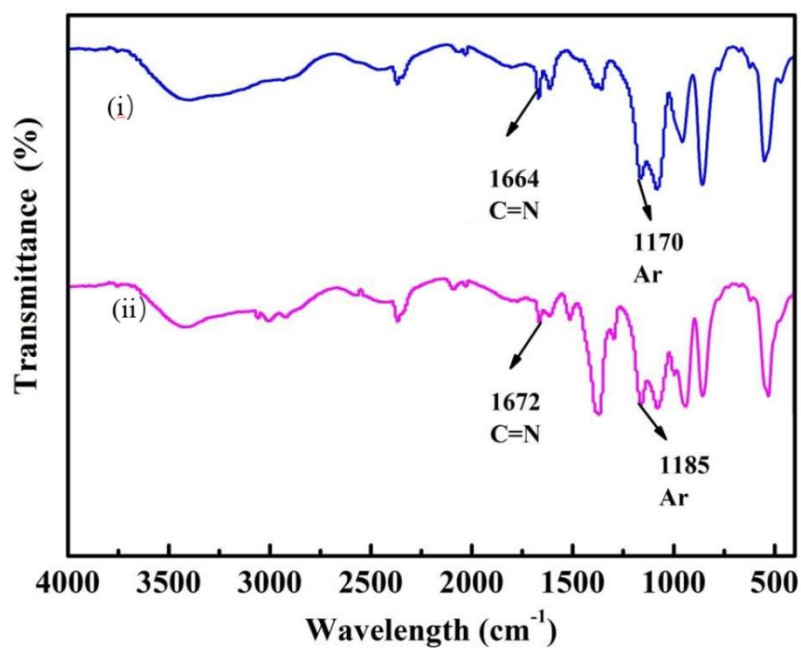


Figure S12: Infrared spectroscopy of **3** (top) and $3 \cdot \text{Cr}^{3+}$ (bottom).

8. Figure of HRMS for 3

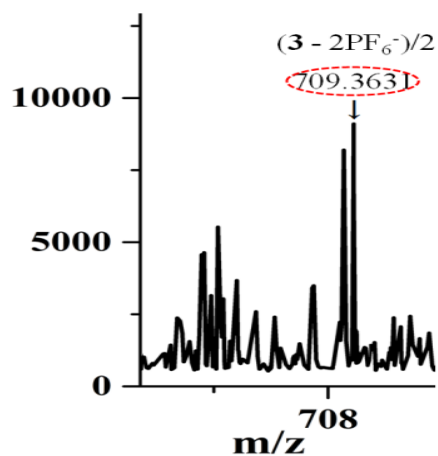


Figure S13: HRMS for 3.

9. 1H NMR and ^{13}C NMR spectra of intermediate and compound 3

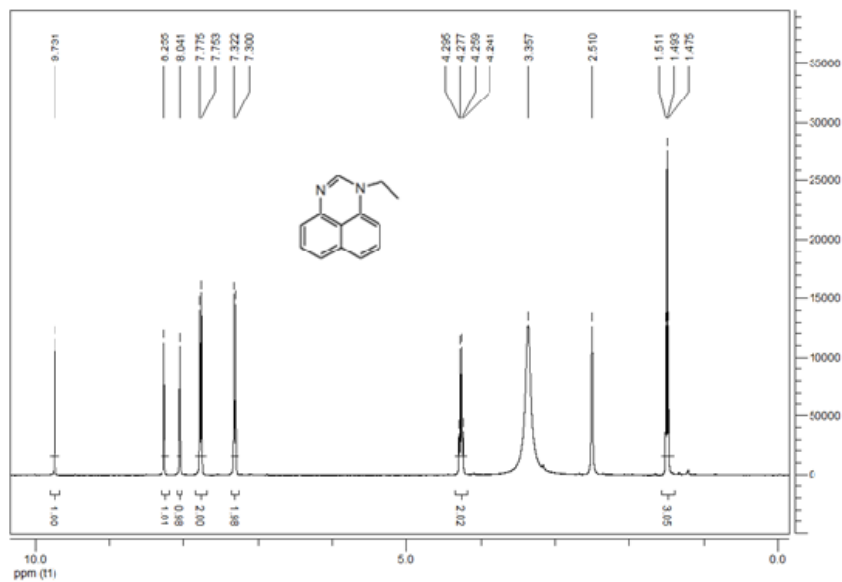


Figure S14: The 1H NMR (400 MHz, $DMSO-d_6$) spectra of 1-ethylperimidinium.

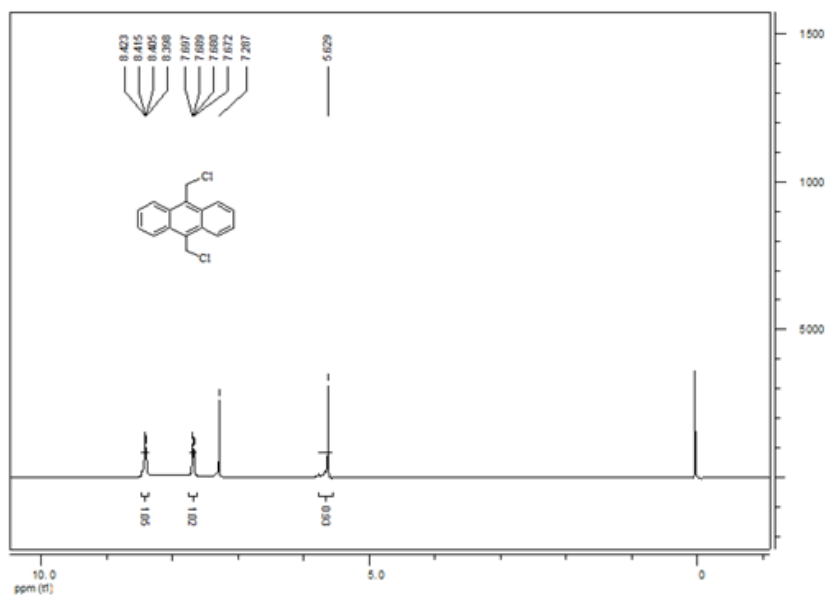


Figure S15: The ¹H NMR (400 MHz, CDCl₃) spectra of 9,10-bis(chloromethyl)anthracene.

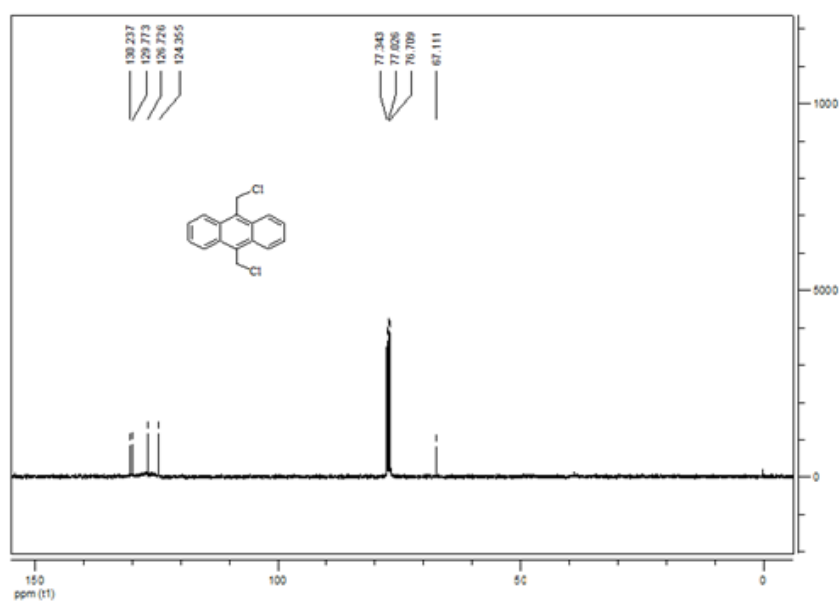


Figure S16: The ¹³C NMR (100 MHz, CDCl₃) spectra of 9,10-bis(chloromethyl)anthracene.

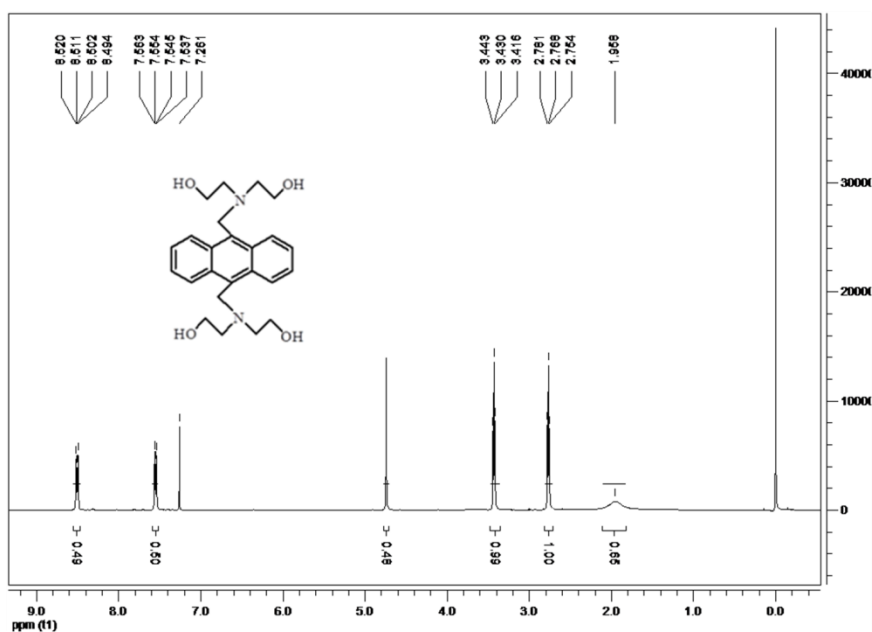


Figure S17: The ^1H NMR (600 MHz, CDCl_3) spectra of 9,10-bis[$\{N,N$ -di(2-hydroxyethyl)amino}methyl]anthracene.

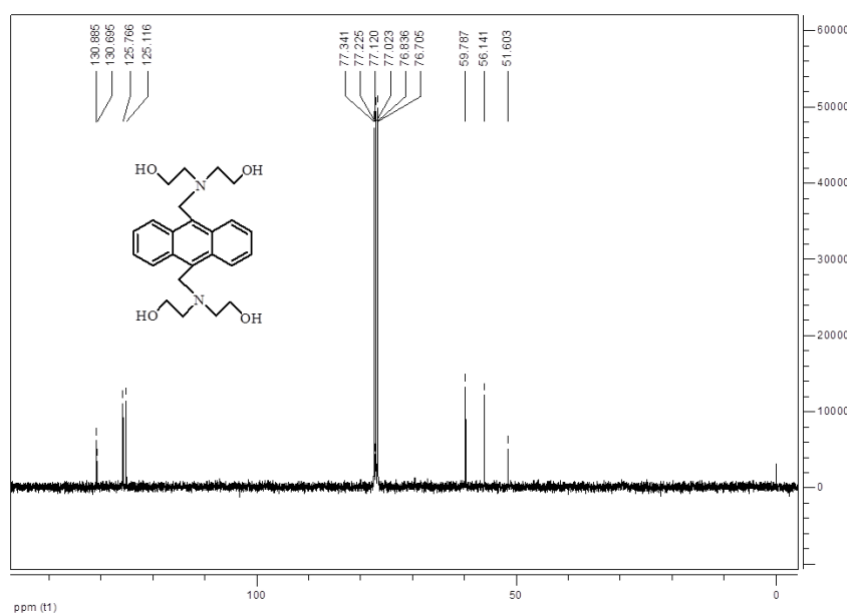


Figure S18: The ^{13}C NMR (150 MHz, CDCl_3) spectra of 9,10-bis[$\{N,N$ -di(2-hydroxyethyl)amino}methyl]anthracene.

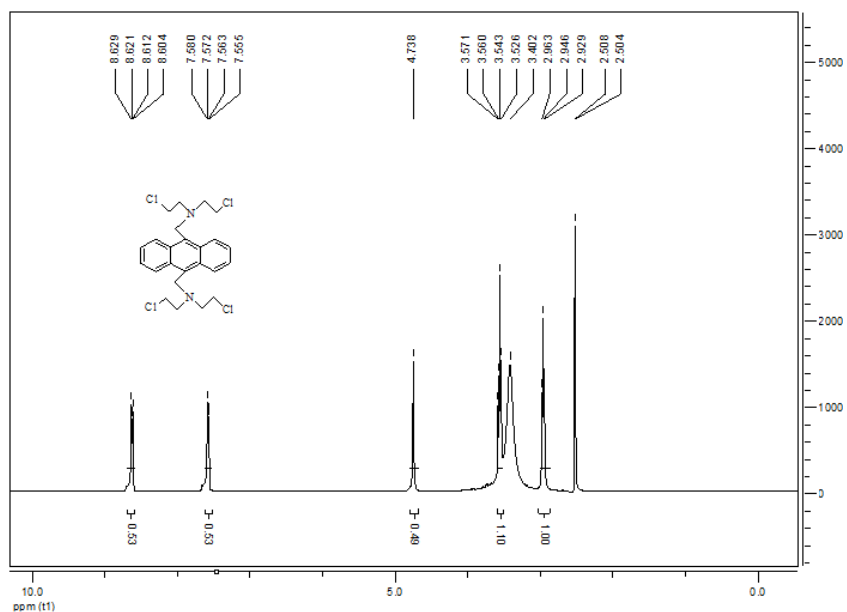


Figure S19: The ¹H NMR (600 MHz, DMSO-*d*₆) spectra of 9,10-bis[*N,N*-di(2-chloroethyl)amino}methyl]anthracene.

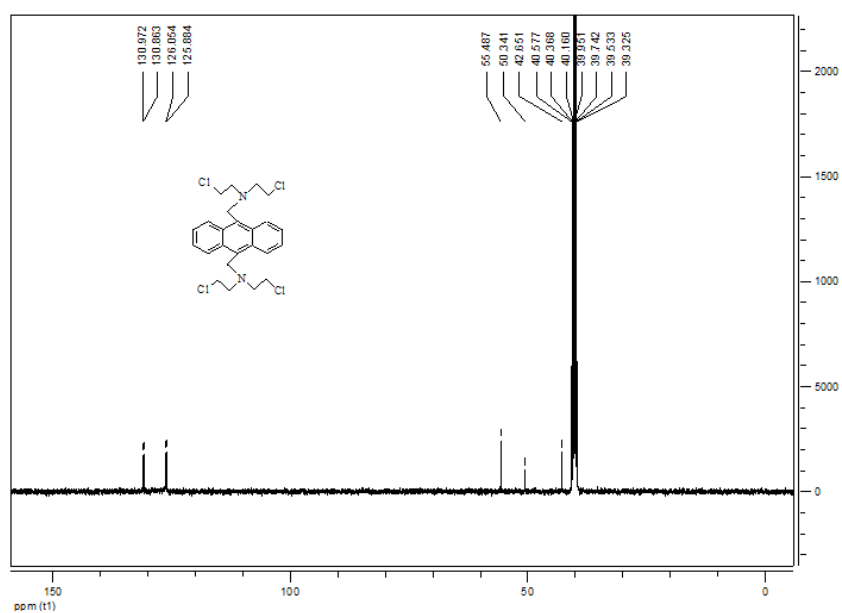


Figure S20: The ¹³C NMR (150 MHz, DMSO-*d*₆) spectra of 9,10-bis[*N,N*-di(2-chloroethyl)amino}methyl]anthracene.

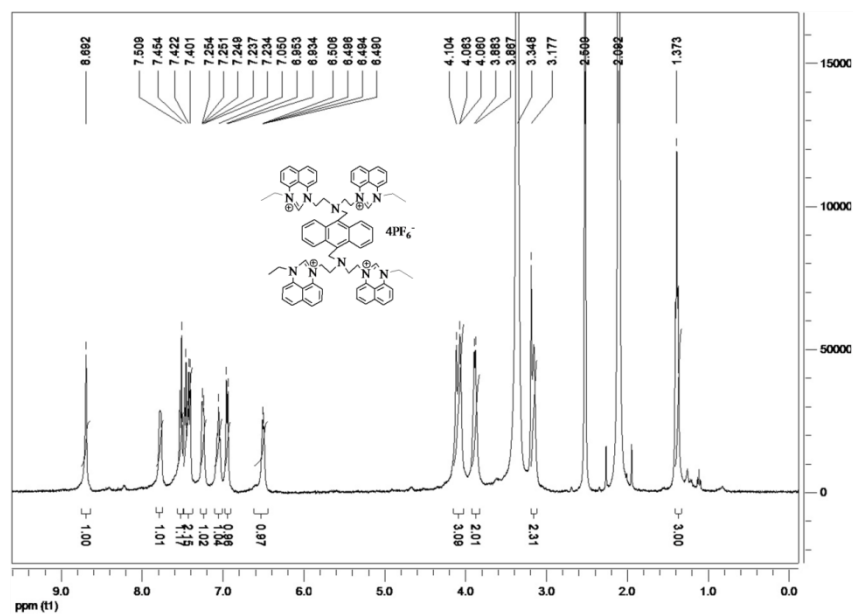


Figure S21: The ^1H NMR (600 MHz, $\text{DMSO}-d_6$) spectrum of **3**.

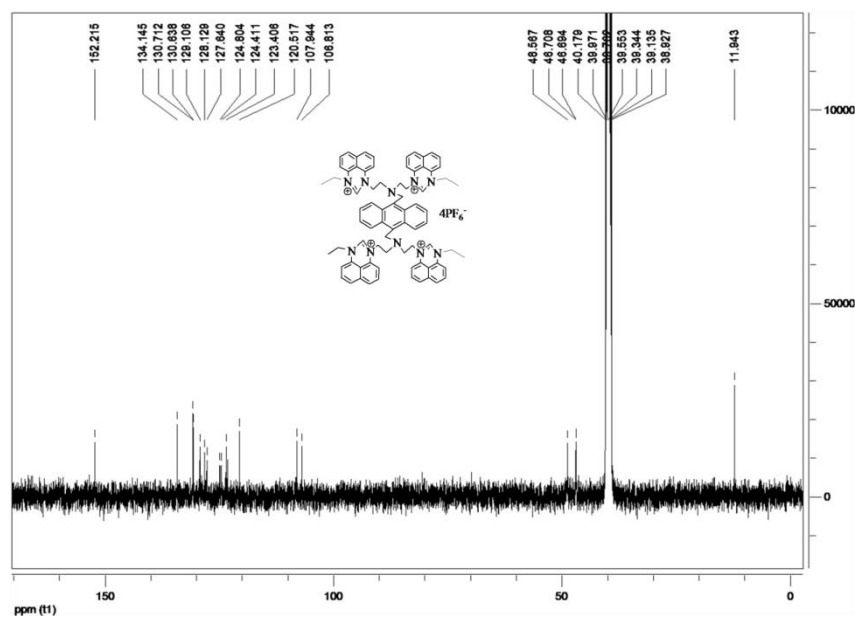


Figure S22: The ^{13}C NMR (150 MHz, $\text{DMSO}-d_6$) spectrum of **3**.